Chapter 11

Ion-Irradiation-Induced Carbon Nanostructures in Optoelectronic Polymer Materials

Taras S. Kavetskyy and Andrey L. Stepanov

Additional information is available at the end of the chapter

http://dx.doi.org/10.5772/62669

Abstract

The recent results obtained on the ion-irradiation-induced carbon nanostructures in optoelectronic polymer materials exemplified by boron-ion-implanted polymethylmethacrylate (B:PMMA) with an energy of 40 keV, ion doses from 6.25×10^{14} to 5.0×10^{16} ions/cm^2, and current density <2 μA/cm^2 are reviewed. The positron annihilation spectroscopy (slow positron beam spectroscopy based on Doppler broadening of positron annihilation gamma rays as a function of incident positron energy and positron annihilation lifetime at a positron energy of 2.15 keV, and temperature-dependent positron annihilation lifetime spectroscopy), optical UV-visible spectroscopy, Raman spectroscopy, electrical (current–voltage) measurements, and nanoindentation test are chosen as the main experimental tools for the investigation of low-energy ion-induced processes in B:PMMA. The formation of carbon nanostructures is confirmed for the samples irradiated with higher ion fluences (>10^{16} ions/cm^2) and the experimental results of the comprehensive study are found to be in a good agreement with SRIM (stopping and range of ions in matter) simulation results.

Keywords: ion irradiation, optoelectronic materials, boron-ion-implanted polymethylmethacrylate, carbon nanostructures

1. Introduction

Ion implantation is a powerful experimental approach for structural modification of materials. In case of organic media, the interest to ion-irradiated polymers is due to the ion implantation being one of the effective technological methods to turn dielectric polymers into semiconductors [1] as well as to improve surface-sensitive mechanical properties of polymers

for hard-materials applications [2]. Substantial improvements in hardness, wear resistance, oxidation resistance, resistance to chemicals, and electrical conductivity are the main characteristics attained by polymeric materials after their low-to-medium-energy ion implantation [3–7].

The formation of free radicals at lower ion doses ($<10^{16}$ ions/cm^2) and carbonization at higher ion doses ($>10^{16}$ ions/cm^2) in the most polymeric materials are of general concept [8–10]. In particular, the ion irradiation of polymers leads to the scission and cross-linking of polymer chains, formation of volatile low-molecular fragments, and carbonization of the implanted layer. The carbonization process depends strongly on the implantation dose or/ and ion current density. As ion dose increases, the several stages can be distinguished for carbonization to be occurred. The formation of pre-carbon structures, nucleation, and growth of the carbon-enriched clusters, aggregation of the clusters, formation of network of conjugated bonds, and transition to amorphous carbon or graphite-like material are the main stages predicted in literature [8–10]. Despite numerical studies of carbonization processes in polymers, the problem remains to understand better how the carbonaceous phase or carbon nanostructures formed under high-dose ion implantation could be dependent on the type of polymer matrix. In this respect, a lot of efforts have been made by researchers studying the B^+-ion implantation into various polymer matrix such as polycarbonate, Kapton, polyethylene, polyamide, polyimide, poly(ethylene terephthalate), cellulose, polypropylene, polystyrene, polyethersulfone, and others ([2, 4, 5, 11–25] and references therein). At the same time, the B^+-ion implantation into widely used in practice polymer polymethylmethacrylate (PMMA) was not studied so far.

The interest to B^+-ion implantation of polymers is due to formation of buried carbonaceous layer leading to increasing conductivity [20, 23]. Also, B^+-ion implantation into polymeric matrix results in significant increase of surface-sensitive mechanical properties. So, Lee et al. [4] reported the ion-induced improvement in hardness of Kapton irradiated by three different ion species, He, B, and Si at 200 keV to a dose of 3.5×10^{19} ions/m^2, where boron produced the largest improvement in hardness among the three, not following the increasing trend in atomic number.

The selection of PMMA matrix to be used for B^+-ion implantation is due to an importance of this polymer for construction of many optical components (waveguides, lenses, prisms, etc.), lithography, biomedical applications, etc. ([26–30] and references therein). PMMA was also a subject for implantation with Ag^+-ions [9, 31] to fabricate composite structures with silver nanoparticles for plasmonic applications as well as for implantation with C^+, N^+ and Ar^+-ions [29, 30] that may find an extensive application in fabrication of various optoelectronic devices including organic light-emitting diodes, backlight components in liquid crystal display systems, diffractive elements, solar cells, waveguides, microcomponents for integrated optical circuits, etc. The well-known key performance and important characteristics of PMMA such as a long-term stability in outdoor environments, excellent surface hardness, light weight, outstanding transmittance and optical clarity, optical design flexibility and control, etc. [32], and high stability upon positron irradiation at room temperature [33] are also taken into account at the selection of basic polymeric matrix for low-energy ion implantation.

In this chapter, a review of recent results obtained using proper experimental and simulation techniques on the boron-ion-implanted polymethylmethacrylate (B:PMMA) is presented. As a result, the formation of ion-irradiation-induced carbon nanostructures in optoelectronic polymer materials exemplified by B:PMMA is evidently confirmed.

2. Experimental

2.1. Sample preparation and SRIM simulation

The B^+-ion implantation with the energy of 40 keV, doses from 6.25×10^{14} to 5.0×10^{16} ions/cm^2 and current density < 2 μA/cm^2 into the optically transparent PMMA plates (1.2 mm thickness) was performed under a pressure of 10^{-5} Torr at room temperature by an "ILU-3" ion accelerator at the Kazan Physical-Technical Institute (KPTI, Russia) similar to as it was earlier done for Xe^+ and Ag^+ ions [34].

For comparative analysis of depth profiles of implanted ions and introduced vacancies in respect to ion mass, SRIM (stopping and range of ions in matter) simulations were carried out for 40 keV He^+, B^+, O^+, P^+, Cl^+, Cu^+, Ag^+, Xe^+, and Au^+ ions implanted into PMMA using the free of charge software of version SRIM-2013 [35].

2.2. Positron annihilation spectroscopy measurements

Positron annihilation spectroscopy (PAS) measurements with slow positron beam spectroscopy (SPBS) based on Doppler broadening of positron annihilation gamma-rays as a function of incident positron energy and positron annihilation lifetime at constant positron energy were performed at the National Institute of Advanced Industrial Science and Technology (AIST, Japan) [36]. Doppler broadening spectra (*S*–*E* and *W*–*E*) were measured using a slow positron beamline in the range of positron incident energy *E* from 0 to 30 keV. Positron annihilation lifetime spectra at incident positron energy of 2.15 keV were measured by another slow positron beamline using an electron linear accelerator as an intense source of slow positrons. The details of the SPBS measurements are reported elsewhere [36].

PAS measurements with positron annihilation lifetime spectroscopy (PALS) and Doppler broadening of annihilation line (DBAL) techniques in the temperature range of 50–300 K using helium cryostat (Closed Cycle Refrigerator, Janis Research Company, Inc., USA) and vacuum equipment (Pfeiffer Vacuum, HiCUBE, Germany) were carried out at the Institute of Physics, Slovak Academy of Sciences (IPSAS, Slovakia) [37–39]. The samples were measured in the cycles of heating and cooling with step of 20 K and elapsed time of 4–5 hours per point. At the selected temperatures, the elapsed time was extended for better statistics in the lifetime spectra. For these temperatures, the continuous lifetime analysis technique to obtain the distributions of *ortho*-positronium (*o*-Ps) lifetime (free-volume voids) was employed using maximum entropy lifetime (MELT) program [40]. The positron annihilation lifetime spectra were taken by the conventional fast-fast coincidence method using plastic scintillators coupled to photomultiplier tubes as detectors. The radioactive ^{22}Na positron source (1.5 MBq activity) was

deposited in an envelope of Kapton foils and then sandwiched between two samples. This source-sample assembly was placed in a vacuum chamber between two detectors to acquire lifetime spectra at different temperatures. The time resolution (FWHM) of positron lifetime spectrometer was 0.32 ns, measured by defect free Al sample as a standard. Analysis of lifetime spectra was carried out using the PATFIT-88/POSITRONFIT [41] software package with proper source corrections. Three component fitting procedure for PALS data treatment was applied and long-lived lifetime component τ_3 and its intensity I_3, ascribing to the *o*-Ps pick-off annihilation in free-volume spaces, was finally taken into account for analysis. Simultaneously with PALS measurements, the DBAL spectra were recorded using a high-purity Ge detector with energy resolution of 1.9 keV FWHM at the energy 1274 keV. The annihilation line was deconvoluted by Gold algorithm that allows eliminating a linear instability of the measuring equipment if the 1274 keV ^{22}Na peak is measured simultaneously with the annihilation peak, for deconvolution of annihilation peak 511 keV; this procedure permits the measurement of small changes of the annihilation peak with high confidence [42]. The Doppler *S* and *W* parameters were used for analysis of a shape of deconvoluted annihilation peak 511 keV. Their numerical values were defined as the ratio of the central area to the total area of the photon peak for *S* parameter and as the ratio of wings area to the total area of the photon peak for *W* parameter.

2.3. Optical spectroscopy measurements

Optical UV-visible spectroscopy measurements were performed using a SHIMADZU-UV 3100PC spectrophotometer in the range of 200–800 nm at AIST, Japan [36].

2.4. Raman spectroscopy measurements

Room temperature Raman spectra were recorded using a Renishaw Raman inVia Reflex spectrometer in the 400–3800 cm^{-1} range with a spectral resolution of ≤1 cm^{-1} [43]. The 514 nm Modu-Laser Stellar-REN Pro 514/50 Argon Laser and 785 nm Near Infrared Diode Laser lines were applied as the excitation source. In order to avoid heat-induced effects, the laser power was set at 10 mW. A standard calibration of wavenumber scale with Si plate was used. The Raman spectroscopy measurements were performed at The John Paul II Catholic University of Lublin (KUL, Poland).

2.5. Electrical measurements

The electrical measuring system was developed at the IPSAS (Slovak Republic) [43]. The measurement of current vs. voltage (*I*–*V*) by transient method or DC method was used in this experiment. The method was selected to check simply presence of the conductivity layer in the material studied. The measuring system includes a cryostat with sample, resistor heating, thermocouple, CSP (charge sensitive preamplifier), excitation circuit of sample, preamplifier, power supply, DAQ (data acquisition) card, and PC (personal computer). The NI PCI 6229 DAQ card was applied [44]. The electrical DC measurement setup used and detail description of basic parameters are reported elsewhere [43].

http://dx.doi.org/10.5772/62669

2.6. Nanoindentation test

Nanoindentation test was carried out using an ultra nano hardness tester (UNHT) with a diamond Berkovich indenter at the Lublin University of Technology (LUT, Poland) [45, 46]. Advantages of the new UNHT design applied for nanoindentation test compared to the conventional nano indenter (or NHT) design, both developed by CSM Instruments (Switzerland) [47], allow us to make measurements with high performance. The UNHT experiment was done in a progressive multicycle mode. The details of the progressive multicycle mode parameters used are reported elsewhere [45].

3. Results and discussion

3.1. SRIM simulation data

Figure 1 shows the typical SRIM simulation results for B^+-implantation into PMMA at energy of 40 keV [36, 45]. Numerical values of SRIM simulation for 40 keV He^+, B^+, O^+, P^+, Cl^+, Cu^+, Ag^+, Xe^+, and Au^+ ions into PMMA are gathered in **Table 1** [48].

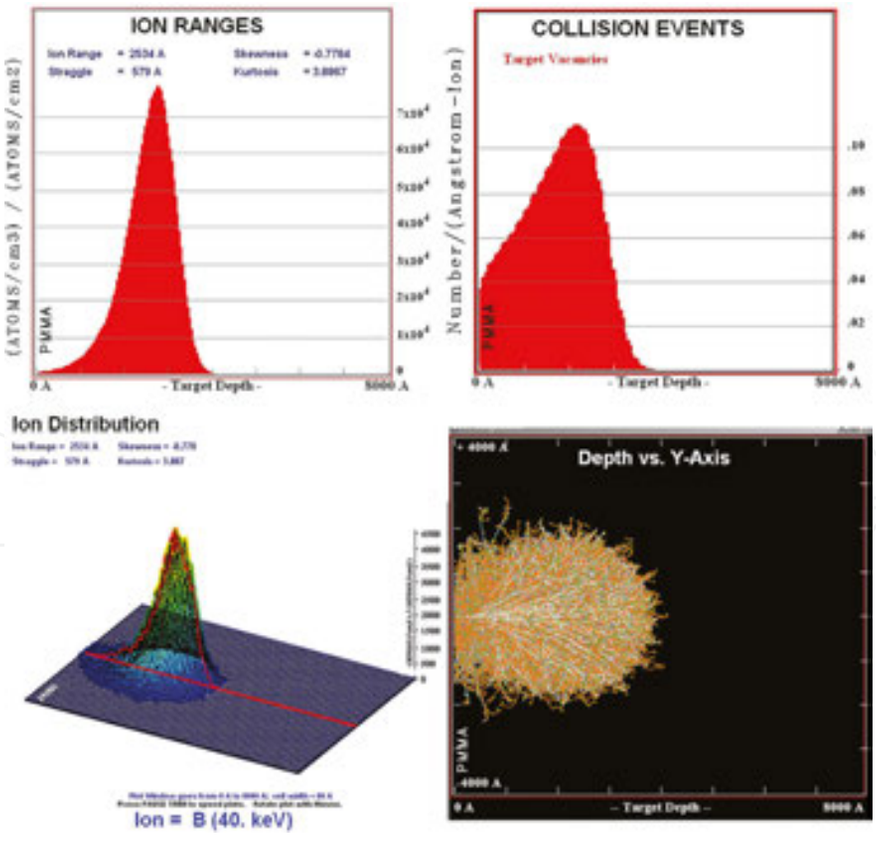

Figure 1. Depth profiles of implanted ions (top, left), introduced vacancies (top, right), 3D image of ion distribution (bottom, left) and depth vs. Y-axis (bottom, right) for B:PMMA. Adapted from [36, 45].

Ion	[b]Atomic weight	[c]R_{max}^{Ion}, nm	R_p^{Ion}, nm	ΔR_p^{Ion}, nm	[c]R_{max}^{V}, nm	[c]R_p^{V}, nm
He^+	4.0026	880	593	102	820	560
[a]B^+	10.81	400	253	58	380	220
[a]O^+	15.999	300	169	45	280	150
P^+	30.974	200	99	29	190	70
Cl^+	35.45	160	85	23	170	60
Cu^+	63.546	130	69	18	140	40
Ag^+	107.87	100	56	11	95	35
Xe^+	131.29	90	56	10	90	30
[a]Au^+	196.97	75	54	7	60	25

Table 1. SRIM simulation results for 40 keV ion implantation into PMMA ([a]data from the work [36]; [b]data from www.webelements.com; [c]data are estimated with error ± 5 nm) [48].

The SRIM data, presented in **Table 1**, were used for estimation a predicted thickness of implanted layer [48]. Let us to explain it on the example of the modified PMMA by 40 keV accelerated B^+ ions. A mean penetration range (R_p^B) is about 253 nm with a longitudinal straggling (ΔR_p^B) of 58 nm in the Gaussian depth distribution. The assumed predicted thickness of the modified PMMA surface layer ($R_p^B + 2\Delta R_p^B$) is about 369 nm, and the maximum penetration depth (R_{max}^B) is about 400 nm. At the same time, the vacancy distribution gives a maximum damage around $R_p^{V,B} = 220$ nm and maximum depth up to around $R_{max}^{V,B} = 380$ nm. Thus, the estimations performed for various ions, listed in **Table 1**, indicate the possible modification of PMMA surface upon low-energy ion implantation in dependence on the ion mass. These values could also be useful in practice for evaluation of geometrical parameters of ion-implanted layers in PMMA matrix.

3.2. Positron annihilation spectroscopy data

The 40 keV B:PMMA polymers with different ion doses have been studied for the first time using PAS techniques such as SPBS [36] and temperature-dependent PALS [37].

SPBS, often called variable-energy PAS, is a powerful experimental tool widely used for evaluation of defects in solids as a function of depth (defect depth profiling) by varying the positron energy in the range of a few eV to tens keV (for review, see Ref. [49]). Thus, SBPS could be a very effective for the detection of defects induced by ion implantation, which are localized near the surface of material. At first, the un-implanted PMMA and implanted B:PMMA were characterized by Doppler broadening of annihilation gamma rays (or DBAL) as a function of incident positron energy in the range of 0–30 keV. And then, using Doppler broadening results, the PAL spectra at incident positron energy of 2.15 keV were measured and analyzed for the investigated samples. **Figure 2** shows the typical variable-energy DBAL and PAL results obtained, the explanation of which has been done in [36].

http://dx.doi.org/10.5772/62669

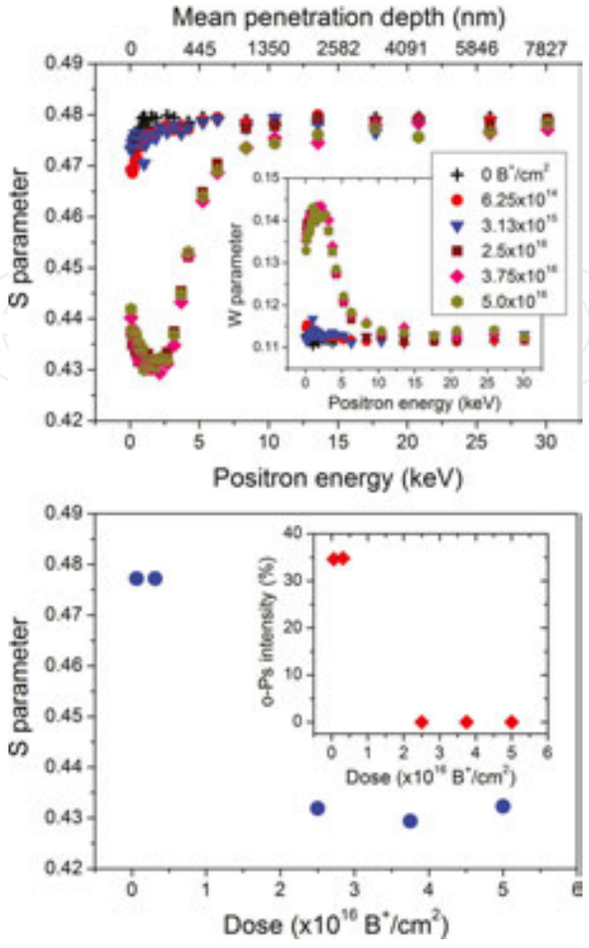

Figure 2. Dose dependence of Doppler *S* and *W* parameters as a function of incident positron energy in the range of 0–30 keV (top) and *S* parameter and *o*-Ps intensity at incident positron energy of 2.15 keV (bottom) for B:PMMA. The error bars are within the size of the symbol. Adapted from [36].

It should only be emphasized here that there are two different processes seen from the *S*-*E* and *W*-*E* curves in dependence on the ion implantation dose [36]. In particular, (i) $S(E)$ increases and $W(E)$ decreases at lower fluences (6.25×10^{14}–3.13×10^{15} ions/cm^2), while (ii) $S(E)$ decreases and $W(E)$ increases at higher fluences (2.5×10^{16}–5.0×10^{16} ions/cm^2) in the range up to 400 nm in a good agreement with the maximum penetration depth R_{max}^{B} = 400 nm after SRIM simulation; positron energy of 2–3 keV, showing the extreme values of $S(E)$ and $W(E)$, corresponds to a mean depth of 100–200 nm in consistent with the maximum damage $R_p^{V,B}$ = 220 nm after SRIM simulation (**Figure 2**, top). A mean penetration depth of positrons (z_m) was estimated as $z_m = (40/\rho)E^n$, where z_m is presented in nm, E the positron energy in keV, ρ is the density (1.18 g/cm^3 for PMMA), and n = 1.6 [50]. The results of variable-energy DBAL and PAL measurements at incident positron energy of 2.15 keV were found to be in consistence (**Figure 2**, bottom) [36]. That is, the decreasing suddenly the $S(E)$ values and an absence of any observable *o*-Ps yield (intensity I_3 ~ 0) for the implanted samples at higher ion doses were detected to be explained due to carbonization effect, taking into account that no *o*-Ps yield has been observed in carbon-based materials such as, for instance, fullerene C_{60} cage [51] and carbon molecular sieve membranes [52].

Thus, the expected two processes of polymer structure modification upon low-energy ion implantation—formation of free radicals at lower fluences (< 10^{16} ions/cm^2) and carbonization at higher fluences (>10^{16} ions/cm^2)—are plausibly confirmed [36].

The results of temperature dependent PALS measurements of the investigated pristine PMMA and implanted B:PMMA samples at lower ion dose (3.13 × 10^{15} ions/cm^2) and at higher ion dose (3.75 × 10^{16} ions/cm^2) are demonstrated in **Figure 3**. The detail description and possible explanation of these data have been presented in [37]. Two structural transitions in the vicinity of ~150 and ~250 K, ascribed to γ and β transitions, respectively, should be noted here, which are observed in the both PMMA and B:PMMA. These structural transitions are found to be in consistent with reference data for PMMA [53, 54].

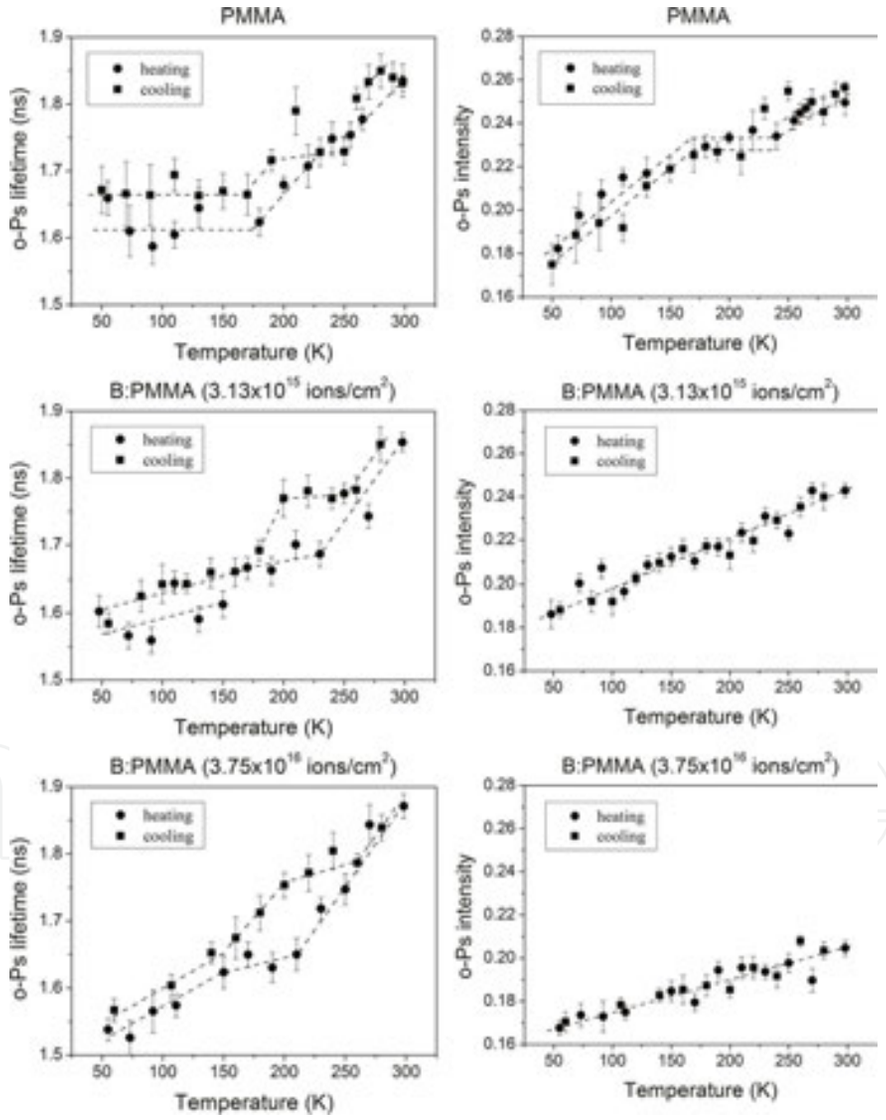

Figure 3. *o*-Ps lifetime and intensity as a function of temperature in the range of 50–298 K for (top) PMMA, (middle) B:PMMA (3.13 × 10^{15} ions/cm^2), and (bottom) B:PMMA (3.75 × 10^{16} ions/cm^2). The dashed lines are drawn as a guide for the eye. Adapted from [37].

http://dx.doi.org/10.5772/62669

The threshold temperatures nearby ~150 and ~250 K for PMMA are also detected on Doppler parameters S/S_0 vs. W/W_0 at different temperatures, normalized to the S_0 and W_0 values at room temperature, using low-temperature DBAL measurements [39] as shown in **Figure 4**. The observed correlation in temperature dependences of S and W parameters and o-Ps data (see **Figure 3**) is found to be in a good agreement with literature PALS and DBAL data for PMMA as well [33].

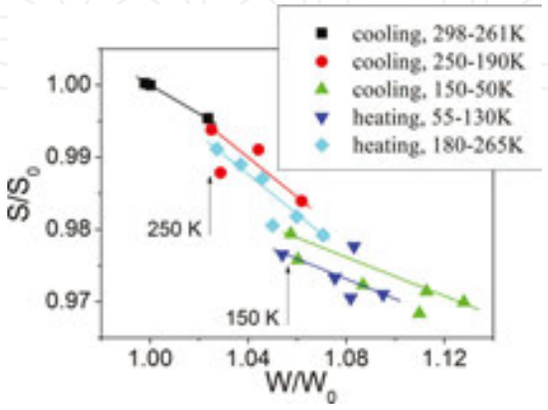

Figure 4. The normalized parameters S/S_0 vs. W/W_0 at different temperatures in the cycles of heating and cooling for PMMA. The solid lines are drawn as a guide for the eye. Adapted from [39].

New results are also obtained from the PALS study of B:PMMA on the free-volume voids distribution at room temperature [37] as shown in **Figure 5**. Namely, estimating the distribution of o-Ps lifetime (or the distribution of free volume detected by o-Ps) by MELT program similarly as it has been done in work [55], it is found that B^+-ion implantation leads to the shortening the lifetime distribution and decreasing molecular weight in PMMA at lower ion dose (3.13×10^{15} ions/cm^2), while at higher ion dose (3.75×10^{16} ions/cm^2) the broadening the lifetime distribution is probably caused by local destruction of PMMA matrix and generation of additional free volumes.

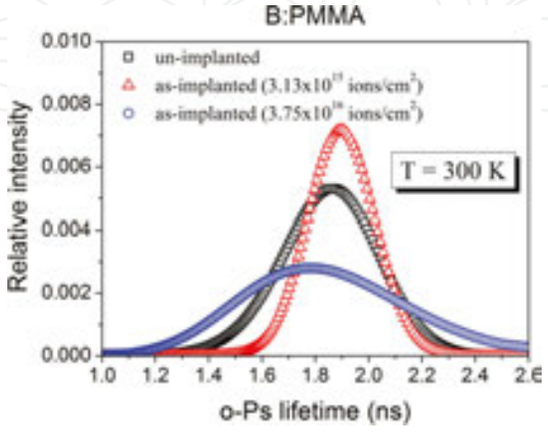

Figure 5. o-Ps lifetime distributions in B:PMMA at different ion doses at room temperature. Adapted from [37].

3.3. Optical spectroscopy data

Application of UV-visible optical absorption spectroscopy for investigation of ion-implanted polymeric materials has already been reported for the Ag^+-implanted PMMA, ORMOCER, and Epoxy resin [31, 34, 56–59] as well as for the C^+, N^+, and Ar^+-implanted PMMA [29, 30]. It has been suggested by the authors that ion irradiation creates compact carbonaceous clusters in polymers, which may also be responsible for a narrowing of optical band gap, enhanced electrical conductivity, and increasing optical absorbance (for example, see [31, 34, 56]). In the case of the investigated B:PMMA, it is found the gradual increase of absorbance at lower fluences (<10^{16} ions/cm^2) and saturation of absorbance at higher fluences (>10^{16} ions/cm^2) as shown in **Figure 6** [36].

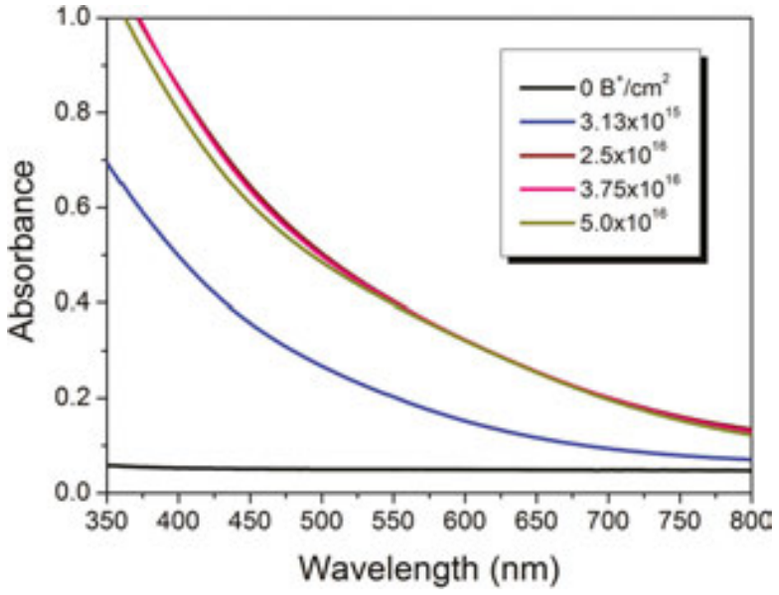

Figure 6. The UV-visible optical absorption spectra of B:PMMA. Adapted from [36].

The observed increasing absorbance for the B:PMMA samples in the course of the ion implantation should be also interpreted as the signature on the formation of carbonaceous clusters which are plausibly confirmed by slow positrons [36].

3.4. Raman spectroscopy data

Figure 7 shows the Raman spectra of the investigated samples excited by 514 nm and 785 nm diode laser lines [43]. Identification of the observed Raman bands has been reported in [43]. The ion-irradiation-induced structural changes as revealed from Raman study can be summarized as follows. New C=C and C−C bands in the vicinity of ~1590 and 1322 cm^{-1}, respectively, are formed for the as-implanted samples at higher fluences (>10^{16} ions/cm^2). At the same time, the decreasing intensity of CH_2 band at ~815 cm^{-1}, C=O band at ~1730 cm^{-1}, O−CH_3 band at ~991 and 2845 cm^{-1}, and C−H band at ~1455, 2955, and 3001 cm^{-1} is detected.

http://dx.doi.org/10.5772/62669

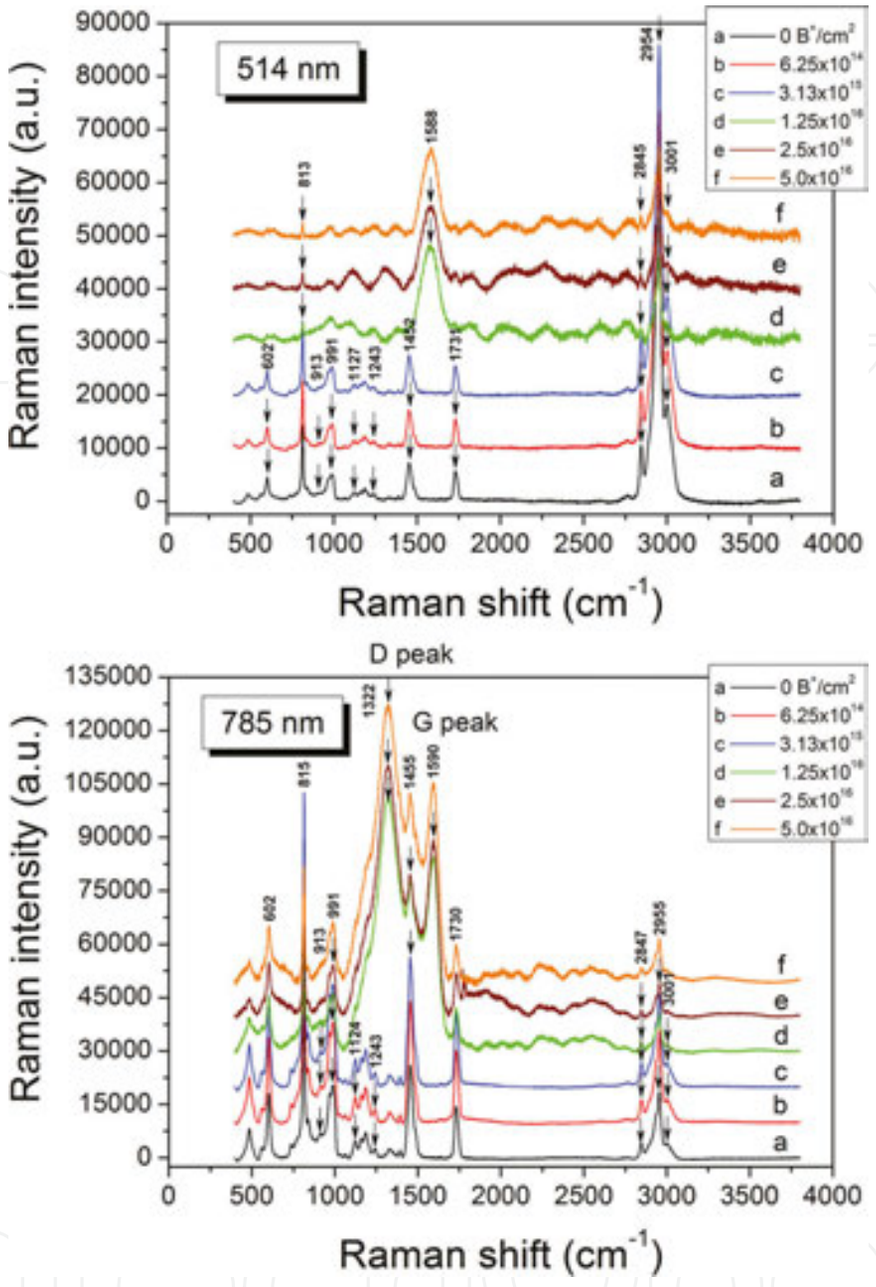

Figure 7. Raman spectra of PMMA and B:PMMA for ion doses from 6.25×10^{14} to 5.0×10^{16} ions/cm^2 excited by (top) 514 nm and (bottom) 785 nm laser lines. Adapted from [43].

In particular, Raman spectroscopy data for excitation by the laser wavelength of 785 nm seem to be additional confirmation for the carbonization processes in the B:PMMA. Indeed, new Raman bands at ~1325 and 1590 cm^{-1}, attributed to C–C and C=C vibrations, respectively, are detected only for the ion-irradiated samples with higher fluences (>10^{16} ions/cm^2). These two new Raman bands may also be attributed to the so-called D and G peaks in the region of 1300-1600 cm^{-1} which are the main peaks characteristic for graphite and graphene structure [60–66]. The intensity ratio of the D and G peaks I_D/I_G is a measure of the size of the sp^2 phase organized in rings [67]. The sp^2 phase is mainly organized in chains, when I_D/I_G is negligible

[63]. The relation between I_D/I_G and the size of the sp^2 phase L_a is given by the equation of Tuinstra and Koenig [60]: $I_D/I_G = C(\lambda)/L_a$. Here, $C(\lambda)$ is a wavelength dependent factor [29, 68]: $C(\lambda) = -126 + 0.033\lambda$, where λ is the excitation wavelength in (Å) at which the Raman spectra were recorded.

A correlation between slow positron beam and Raman spectroscopy results for B:PMMA is mentioned in our recent works [69]. **Table 2** gives the SPBS data, exemplified by *o*-Ps lifetimes and intensities at incident positron energy of 2.15 keV and Raman data, exemplified by I_D/I_G and L_a, for the same B:PMMA samples. A good correlation between these data is clearly observed. Thus, the expected carbonization processes or formation of carbon nanostructures at higher fluences (>10^{16} ions/cm^2) can independently be identified using SPBS and Raman spectroscopy, providing their combination as a powerful experimental tool in the investigation of ion-implanted polymers.

Dose [B^+/cm^2]	*o*-Ps lifetime, τ_3 [ns]	*o*-Ps intensity, I_3 [%]	I_D/I_G	L_a [nm]
0	1.765	35.0	No peaks	
6.25×10^{14}	1.752	34.6	No peaks	
3.13×10^{15}	1.752	34.8	No peaks	
2.5×10^{16}		No *o*-Ps or ~0	1.42	9.4
5.0×10^{16}		No *o*-Ps or ~0	1.40	9.5

Table 2. *o*-Ps lifetimes and intensities at incident positron energy of 2.15 keV and the intensity ratio of the D and G peaks, and calculated sizes of sp^2 phase L_a [69].

3.5. Electrical measurements data

The un-implanted PMMA and as-implanted B:PMMA samples were measured at 300 K and 360 K with DC method [43]. It was supposed that the conductive layer in ion-implanted polymer is dependent on the temperature and at a higher temperature the effect of increasing conductivity with temperature will be more pronounced. In order to avoid a possible structural change in polymer matrix, the maximum temperature at 360 K was selected in the electrical measurement experiment, not exceeding the glass transition temperature T_g of PMMA ranging from 358 to 438 K; the range is so wide because of the vast number of commercial compositions which are copolymers with co-monomers other than methyl methacrylate [70]. Similar value $T_g \cong 355 \pm 18$ K of PMMA was obtained using temperature dependent positron annihilation lifetime measurements [53].

Figure 8 shows the obtained *I-V* dependences, fitted by the linear regression line [43]. As an example, the *I-V* characteristic of as-implanted B:PMMA (5.0×10^{16} ions/cm^2) sample is presented with noise (as-implanted + noise (II)) and linear regression line (linear fit of as-implanted (II)). While for other samples only, the linear regression lines of the DC measurements are demonstrated. More details of the electrical measurement experiment have been reported in [43].

http://dx.doi.org/10.5772/62669

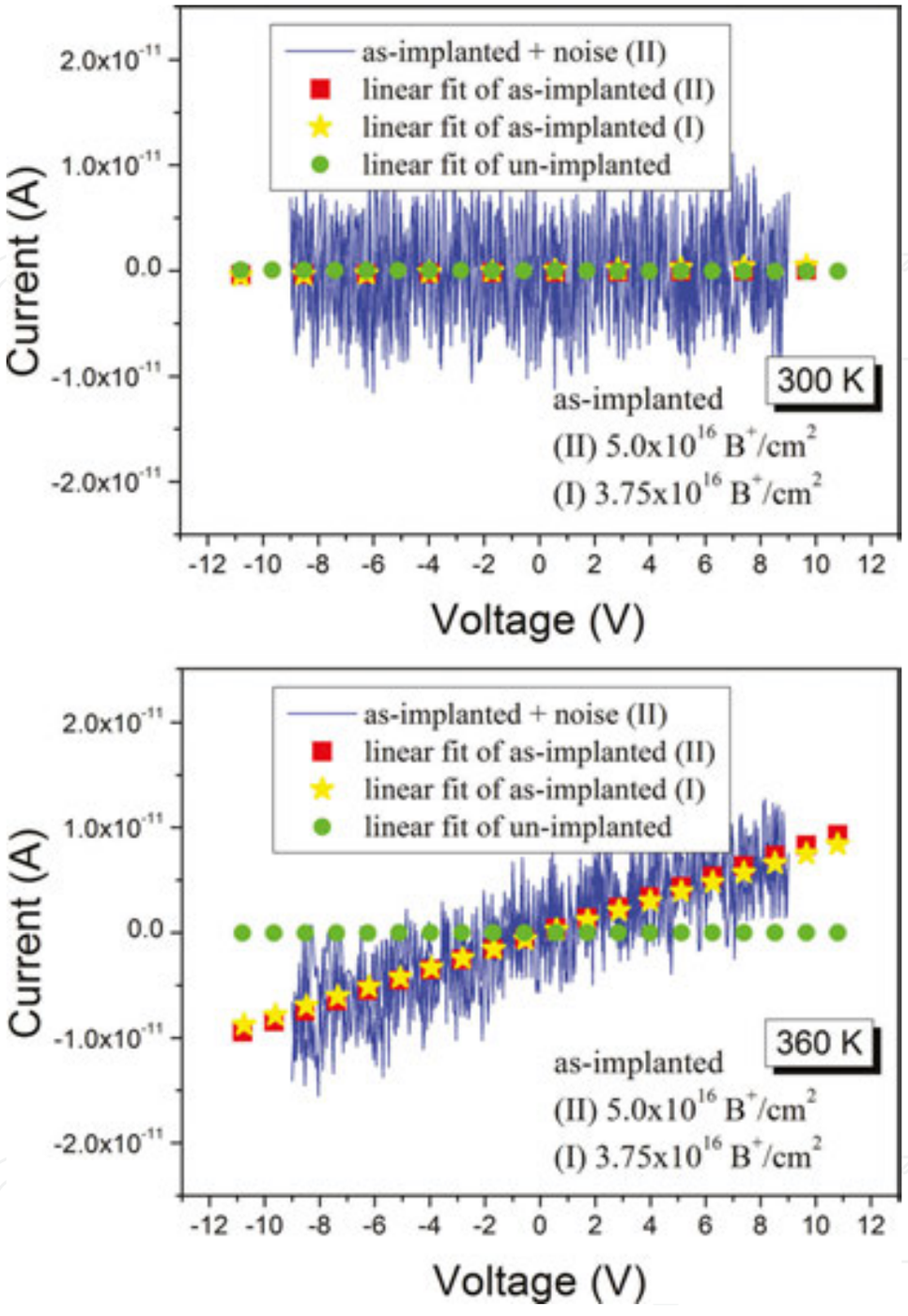

Figure 8. *I-V* dependences for PMMA and B:PMMA (3.75×10^{16} and 5.0×10^{16} ions/cm^2) at temperatures (top) 300 and (bottom) 360 K. Adapted from [43].

The numerical values of the *I-V* characteristics are presented in **Table 3** [43]. It is evidently proven that the pristine PMMA does not exhibit any conductivity neither at higher temperature applied. At room temperature, the slope of linear regression line of *I-V* dependence remains unchanged and has even negative value. In contrary to unimplanted sample, the results of the *I-V* measurements for the B:PMMA (3.75×10^{16} and 5.0×10^{16} ions/cm^2) samples

revealed the change of slope of the linear regression line of *I-V* dependence at 360 K. It means that the as-implanted samples have created a very thin conductive layer or conductive joints due to carbonization processes or formation of carbon nanostructures in consistent with the results of slow positron beam and Raman spectroscopy measurements [36, 43].

Parameters of linear regression	**Temperature 300 K**		
	PMMA	**B:PMMA (3.75×10^{16} ions/cm^2)**	**B:PMMA (5.0×10^{16} ions/cm^2)**
Slope	−5.85E-15	4.79E-14	2.18E-14
Error	2.64E-14	2.64E-14	3.56E-14
CC	0.008	0.07	0.02
SD	3.59E-12	3.68E-12	4.98E-12
Parameters of linear regression	**Temperature 360 K**		
	PMMA	**B:PMMA (3.75×10^{16} ions/cm^2)**	**B:PMMA (5.0×10^{16} ions/cm^2)**
Slope	2.88E-16	7.96E-13	8.68E-13
Error	1.62E-15	2.71E-14	2.53E-14
CC	0.007	0.73	0.79
SD	2.77E-13	3.77E-12	3.53E-12

Table 3. The evaluated values of *I-V* measurements of PMMA and B:PMMA with higher fluences (3.75×10^{16} and 5.0×10^{16} ions/cm^2) at temperatures 300 and 360 K: Slope is value of slope of line of linear regression, Error is the error of linear regression, CC is correlation coefficient, and SD is standard deviation of the linear regression [43].

3.6. Nanoindentation test data

A first time the results of investigation of the influence of low dose (6.25×10^{14} ions/cm^2) B^+-ion-irradiation on the mechanical properties (hardness and elastic modulus) of PMMA probed by nanoindentation with UNHT in the range of 300–1100 nm indentation depth have been reported in [45]. It has been established that the hardness and elastic modulus versus maximum indentation depth illustrate the main difference between the un-implanted (pristine) and ion-implanted samples in the range up to about 400 nm. The same value of the maximum penetration depth of B^+-ions into PMMA has been found using SPBS and SRIM simulation [36]. As a continuation of the nanoindentation test of the B:PMMA, the averaged values of indentation hardness versus maximum indentation depth for the un-implanted and as-implanted samples with ion doses of 6.25×10^{14}, 1.25×10^{16}, 2.5×10^{16}, and 3.75×10^{16} ions/cm^2 are plotted in **Figure 9** [46].

http://dx.doi.org/10.5772/62669

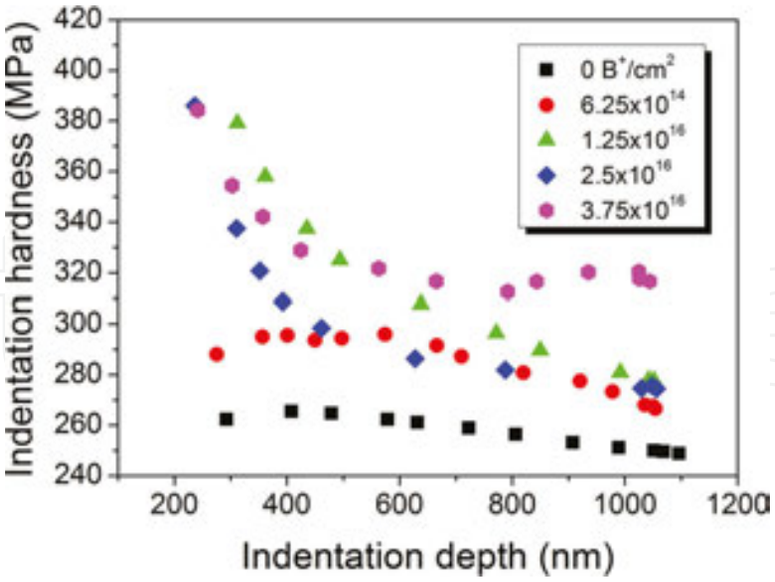

Figure 9. Indentation hardness versus maximum indentation depth for PMMA and B:PMMA (6.25×10^{14}, 1.25×10^{16}, 2.5×10^{16}, and 3.75×10^{16} ions/cm^2). Adapted from [46].

One may see that the hardness dependence on the maximum indentation depth demonstrates the difference between the PMMA and B:PMMA samples in the entire range studied up to 1100 nm with the largest changes in the vicinity of 300-400 nm in consistence with the maximum penetration depth of B^+-ions into PMMA as revealed from SPBS measurements and SRIM simulation [36]. The observed improving of surface-sensitive mechanical properties of B:PMMA by ion beam processing is obviously detected to be more significant as ion dose increases, that may be suitable for hard-materials applications. According to Lee et al. [4] these properties are apparently related to the effectiveness of cross-linking. Besides, the abovementioned formation of carbon nanostructures upon high-dose ion implantation (>10^{16} ions/cm^2) seems to be also important. But further increase of hardness with deeper penetration of indenter up to 1100 nm for higher fluences (3.75×10^{16} B^+/cm^2) was found to be very interesting and not fully understood yet (see **Figure 9**). Actually, similar results that the hardness of B^+-implanted polycarbonate increased with increasing ion dose has also been observed in Ref. [2] but only for penetration of indenter up to 400 nm, that is not so far from the implanted layer as in our case. A deeper understanding the low-energy ion-irradiation-induced processes in polymeric materials exemplified by PMMA irradiated by accelerated light, middle, and heavy ions is still required.

4. Conclusions

The formation of carbon nanostructures has been confirmed for the B:PMMA samples irradiated with higher ion fluences (>10^{16} ions/cm^2) and the experimental results of the comprehensive study have been found to be in a good agreement with SRIM simulation results. It is expected that the results obtained for low-energy B^+-ion implantation into PMMA will

have impact on research and development in the fields of nanoscience, nanotechnology, and nanooptoelectronics, in particular, to be potentially of interest for fabrication of organic luminescent devices, backlight components in liquid crystal display systems, diffractive elements and microcomponents for integrated optical circuits, solar cells, waveguides, etc. similarly as it has been foreseen for low-energy C^+, N^+, and Ar^+-ion implantation into PMMA [29, 30].

Acknowledgements

T.S. Kavetskyy acknowledges the SAIA for scholarships in the Institute of Physics of SAS within the National Scholarship Program of the Slovak Republic. This work was also supported in part by the SFFR of Ukraine (Nos. F40.2/019 and F52.2/003) and MES of Ukraine (Nos. 0114U002616 and 0114U002617). A.L. Stepanov thanks the RFBR (No. 15-48-02525) and RSF (No. 14-13-00758) in Russia for financial support.

Author details

Taras S. Kavetskyy[1,2*] and Andrey L. Stepanov[3,4,5]

*Address all correspondence to: kavetskyy@yahoo.com

1 The John Paul II Catholic University of Lublin, Lublin, Poland

2 Drohobych Ivan Franko State Pedagogical University, Drohobych, Ukraine

3 Kazan Physical-Technical Institute, Russian Academy of Sciences, Kazan, Russian Federation

4 Kazan Federal University, Kazan, Russian Federation

5 Kazan National Research Technological University, Kazan, Russian Federation

References

[1] Wasserman B, Braunstein G, Dresselhaus MS, Wnek GE. Implantation-induced conductivity of polymers. Mater. Res. Soc. Symp. Proc. 1983; 27: 423–428. DOI: 10.1557/PROC-27-423

[2] Lee EH, Rao GR, Mansur LK. Improved hardness and wear properties of B-ion implanted polycarbonate. J. Mater. Res. 1992; 7: 1900–1911. DOI: 10.1557/JMR.1992.1900

[3] Bridwell LB. Ion implantation of polymers for electrical conductivity enhancement. Solid State Phenomena. 1992; 27: 163–180. DOI: 10.4028/www.scientific.net/SSP.27.163

[4] Lee EH, Rao GR, Lewis MB, Mansur LK. Ion beam application for improved polymer surface properties. Nucl. Instr. Meth. B. 1993; 74: 326–330. DOI: 10.1016/0168-583X(93)95070-L

[5] Rao GR, Lee EH, Mansur LK. Structure and dose effects on improved wear properties of ion-implanted polymers. Wear 1993; 162–164: 739–747. DOI: 10.1016/0043-1648(93)90074-V

[6] Goyal PK, Kumar V, Gupta R, Kumar S, Kumar P, Kanjilal D. Effect of Ar+ ion implantation on electrical conductivity of polycarbonate. AIP Conf. Proc. 2011; 1349: 543–549. DOI: 10.1063/1.3605973

[7] Goyal PK, Kumar V, Gupta R, Kumar S, Kumar P, Kanjilal D. Study of electrical conductivity of Kr^+ ion implanted polycarbonate in relation to carbon structure. AIP Conf. Proc. 2011; 1393: 147–151. DOI: 10.1063/1.3653652

[8] Sviridov DV. Chemical aspects of implantation of high-energy ions into polymeric materials. Russ. Chem. Rev. 2002; 71: 315–327. DOI: 10.1070/RC2002v071n04ABEH000710

[9] Stepanov AL. Optical properties of metal nanoparticles synthesized in a polymer by ion implantation: A review. Tech. Phys. 2004; 49: 143–153. DOI: 10.1134/1.1648948

[10] Popok VN. Ion implantation of polymers: Formation of nanoparticulate materials. Rev. Adv. Mater. Sci. 2012; 30: 1–26. http://www.ipme.ru/e-journals/RAMS/no_13012/01_popok.pdf

[11] Fink D, Müller M, Stettner U, Behar M, Fichtner PFP, Zawislak FC, Koul S. Non-regular depth profiles of light ions implanted into organic polymer films. Nucl. Instr. Meth. B 1988; 32: 150–154. DOI: 10.1016/0168-583X(88)90199-1

[12] Guimaraes RB, Amaral L, Behar M, Fichtner PFP, Zawislak FC, Fink D. Implanted boron depth profiles in the AZ111 photoresist. J. Appl. Phys. 1988; 63: 2083–2085. DOI: 10.1063/1.341112

[13] Azarko II, Hnatowicz V, Kozlov IP, Kozlova EI, Odzhaev VB, Popok VN. EPR spectroscopy of ion implanted polymer films. Phys. Stat. Sol. A 1994; 146: K23–K27. DOI: 10.1002/pssa.2211460239

[14] Azarko II, Karpovich IA, Kozlov IP, Kozlova EI, Odzhaev VB, Popok VN, Hnatowicz V. Influence of ion implantation on the properties of polymer films. Solid State Commun. 1995; 95: 49–51. DOI: 10.1016/0038-1098(95)00905-1

[15] Odzhaev VB, Azarko II, Karpovich IA, Kozlov IP, Popok VN, Sviridov DV, Hnatowicz V, Jankovskij ON, Rybka V, Švorčík V. The properties of polyethylene and polyamide

implanted with B+ ions to high doses. Mater. Letters 1995; 23: 163–166. DOI: 10.1016/0167-577X(94)00274-6

[16] Popok VN, Odzhaev VB, Kozlov IP, Azarko II, Karpovich IA, Sviridov DV. Ion beam effects in polymer films: Structure evolution of the implanted layer. Nucl. Instr. Meth. B 1997; 129: 60–64. DOI: 10.1016/S0168-583X(97)00208-5

[17] Vacik J, Cervena J, Fink D, Klett R, Hnatowicz V, Popok V, Odzhaev V. High fluence boron ion implantation into polymers. Radiat. Eff. Def. Solids. 1997; 143: 139–156. DOI: 10.1080/10420159708212955

[18] Kozlov IP, Odzhaev VB, Karpovich IA, Popok VN, Sviridov DV. Optical properties of ion-implanted polymer layers. J. Appl. Spectr. 1998; 65: 390–394. DOI: 10.1007/BF02675458

[19] Kozlov IV, Odzhaev VB, Popok VN, Azarko II, Kozlova EI. Paramagnetic properties of ion-implanted polymer layers. J. Appl. Spectr. 1998; 65: 583–588. DOI: 10.1007/BF02675652

[20] Popok VN, Karpovich IA, Odzhaev VB, Sviridov DV. Structure evolution of implanted polymers: Buried conductive layer formation. Nucl. Instr. Meth. B. 1999; 148: 1106–1110. DOI: 10.1016/S0168-583X(98)00799-X

[21] Vacík J, Hnatowicz V, ČervenáJ, Peřina V, Popok V, Odzhaev V, Fink D. High fluence boron implantation into polyimide. Nucl. Instr. Meth. B 1999; 148: 1126–1130. DOI: 10.1016/S0168-583X(98)00814-3

[22] Vacík J, Hnatowicz V, ČervenáJ, Peřina V, Popok V, Odzhaev V, Švorčík V, Rybka V, Arenholz E, Fink D. Annealing behaviour of boron atoms implanted into polyethyleneterephtalate. Nucl. Instr. Meth. B 2000; 166–167: 637–640. DOI: 10.1016/S0168-583X(99)01049-6

[23] Odzhaev VB, Popok VN, Kozlova EI, Jankovskij ON, Karpovich IA. Electrical properties of polyethylene modified by ion implantation and diffusion. Nucl. Instr. Meth. B 2000; 166–167: 655–659. DOI: 10.1016/S0168-583X(99)01212-4

[24] Popok VN, Odzhaev VB, Azarko II, Kozlov IP, Sviridov DV, Hnatowicz V, Vacík J, ČervenáJ. Multistage ion implantation of polyamide-6 films. Nucl. Instr. Meth. B 2000; 166–167: 660–663. DOI: 10.1016/S0168-583X(99)01211-2

[25] Popok VN, Azarko II, Odzhaev VB, Tóth A, Khaibullin RI. High fluence ion beam modification of polymer surfaces: EPR and XPS studies. Nucl. Instr. Meth. B 2001; 178: 305–310. DOI: 10.1016/S0168-583X(00)00491-2

[26] Kuo SW, Kao HC, Chang FC. Thermal behavior and specific interactions in high glass transition temperature PMMA copolymer. Polymer 2003; 44: 6873–6882. DOI: 10.1016/j.polymer.2003.08.026

[27] Teixeira FS, Salvadori MC, Cattani M, Brown IG. Gold-implanted shallow conducting layers in polymethylmethacrylate. J. Appl. Phys. 2009; 105: 064313-1–064313-5. DOI: 10.1063/1.3088874

[28] Tsvetkova T, Balabanov S, Avramov L, Borisova E, Angelov I, Sinning S, Bischoff L. Photoluminescence enhancement in Si^+ implanted PMMA. Vacuum 2009; 83: S252–S255. DOI: 10.1016/j.vacuum.2009.01.075

[29] Wang J, Zhu F, Zhang B, Liu H, Jia G, Liu C. Photoluminescence and reflectivity of polymethylmethacrylate implanted by low-energy carbon ions at high fluences. Appl. Surf. Sci. 2012; 261: 653–658. DOI: 10.1016/j.apsusc.2012.08.076

[30] Gupta R, Kumar V, Goyal PK, Kumar S. Optical characterization of poly(methyl methacrylate) implanted with low energy ions. Appl. Surf. Sci. 2012; 263: 334–338. DOI: 10.1016/j.apsusc.2012.09.056

[31] Stepanov AL. Optical extinction of metal nanoparticles synthesized in polymer by ion implantation. In: Nicolais L, Carotenuto G, editors. Metal-Polymer Nanocomposites. Italy: Wiley; 2005. p. 241–263. DOI: 10.1002/0471695432.ch8

[32] Colburn P. Acrylic materials in PV applications: Making an informed choice. Evonik Industries – NREL PV Reliability Workshop [Internet]; 2011. Available from: http://www1.eere.energy.gov/solar/pdfs/pvmrw2011_23_cpv_colburn.pdf [accessed 2011-02-17].

[33] Qi N, Chen ZQ, Uedono A. Molecular motion and relaxation below glass transition temperature in poly (methyl methacrylate) studied by positron annihilation. Rad. Phys. Chem. 2015; 108: 81–86. DOI: 10.1016/j.radphyschem.2014.11.018

[34] Stepanov AL, Abdullin SN, Petukhov VY, Osin YN, Khaibullin IB. Formation of metal-polymer composites by ion implantation. Phil. Mag. B 2000; 80: 23–28. DOI: 10.1080/13642810008218336

[35] Ziegler JF, Biersak JP, Littmark U. The Stopping and Range of Ions in Solids. New York: Pergamon; 1996. http://www.srim.org/

[36] Kavetskyy T, Tsmots V, Kinomura A, Kobayashi Y, Suzuki R, Mohamed HFM, Šauša O, Nuzhdin V, Valeev V, Stepanov AL. Structural defects and positronium formation in 40 ke V B^+-implanted polymethylmethacrylate. J. Phys. Chem. B 2014; 118: 4194–4200. DOI: 10.1021/jp410763t

[37] Kavetskyy TS, Tsmots VM, Voloshanska SY, Šauša O, Nuzhdin VI, Valeev VF, Osin YN, Stepanov AL. Low-temperature positron annihilation study of B^+-ion implanted PMMA. Low Temp. Phys. 2014; 40: 747–751. DOI: 10.1063/1.4892646

[38] Kavetskyy T, Tsmots V, Šauša O, Stepanov AL. Structural modification of chalcogenide glasses by gamma-irradiation studied with DBAL technique. Phys. Status Solidi C 2012; 9: 2420–2423. DOI: 10.1002/pssc.201200252

[39] Kavetskyy TS, Tsmots VM, Voloshanska SY, Šauša O, Stepanov AL. Low-temperature Doppler broadening of annihilation line study of PMMA. In: Proceedings of the 6th International Scientific and Technical Conference on Sensor Electronics and Microsystem Technologies (SEMST-6); 29 September–3 October 2014; Astroprint; Odessa; 2014. p. 226.

[40] Shukla A, Peter M, Hoffmann L. Analysis of positron lifetime spectra using quantified maximum entropy and a general linear filter. Nucl. Instr. Meth. A 1993; 335: 310–317. DOI: 10.1016/0168-9002(93)90286-Q

[41] Kirkegaard P, Eldrup M, Mogensen OE, Pedersen NJ. Program system for analysing positron lifetime spectra and angular correlation curves. Comp. Phys. Commun. 1981; 23: 307–335. DOI: 10.1016/0010-4655(81)90006-0

[42] Bandžuch P, MorháčM, Krištiak J. Study of the Van Cittert and gold iterative methods of deconvolution and their application in the deconvolution of experimental spectra of positron annihilation. Nucl. Instr. Meth. A 1997; 384: 506–515. DOI: 10.1016/S0168-9002(96)00874-1

[43] Kavetskyy T, Nowak J, Borc J, Rusnák J, Šauša O, Stepanov AL. Carbonization in boron-ion-implanted polymethylmethacrylate as revealed from Raman spectroscopy and electrical measurements. Spectroscop Lett. 2016; 49: 5–10. DOI: 10.1080/00387010.2015.1044113

[44] National Instruments [Internet]. 2014. Available from: http://www.ni.com/datasheet/pdf/en/ds-15 [accessed 2014-11-06].

[45] Kavetskyy TS, Borc J, Kukhazh YY, Stepanov AL. The influence of low dose ion-irradiation on the mechanical properties of PMMA probed by nanoindentation. In: Petkov P, Tsiulyanu D, Kulisch W, Popov C, editors. Nanoscience Advances in CBRN Agents Detection, Information and Energy Security. NATO Science for Peace and Security Series – A: Chemistry and Biology. The Netherlands: Springer; 2015. p. 65–71. DOI: 10.1007/978-94-017-9697-2_7

[46] Kavetskyy TS, Kukhazh YY, Borc J, Stepanov AL. Nanoindentation of boron-ion implanted polymethylmethacrylate up to 1100 nm indentation depth. In: Proceedings of the XXII International Conference on Ion-Surface Interactions (ISI-2015); 20–24 August 2015; NRNU MEPh I; Moscow; 2015. Vol. 2. p. 132–135.

[47] Introduction on Instrumented Indentation [Internet]. 2013. Available from: http://www.csm-instruments.com [accessed 2013-11-15].

[48] Kavetskyy TS, Stepanov AL. Spectroscopic investigations of ion-induced processes in polymethylmethacrylate at low-energy boron-ion implantation. In: Proceedings of the XXII International Conference on Ion-Surface Interactions (ISI-2015); 20–24 August 2015; NRNU MEPh I; Moscow; 2015. Vol. 3. p. 339–342.

[49] Schultz PJ, Lynn KG. Interaction of positron beams with surfaces, thin films, and interfaces. Rev. Mod. Phys. 1988; 60: 701–779. DOI: 10.1103/Rev Mod Phys.60.701

[50] Kobayashi Y, Ito K, Oka T, He C, Mohamed HFM, Suzuki R, Ohdaira T. Application of positron beams to the study of positronium-forming solids. Appl. Surf. Sci. 2008; 255: 174–178. DOI: 10.1016/j.apsusc.2008.05.278

[51] Krištiak J, Krištiakova K, Šauša O. Phase transition in C_{60} observed by positron annihilation. Phys. Rev. B. 1994; 50: 2792–2794. DOI: 10.1103/Phys Rev B.50.2792

[52] Liao KS, Fu YJ, Hu CC, Chen JT, Lin DW, Lee KR, Tung KL, Jean YC, Lai JY. Microstructure of carbon molecular sieve membranes and their application to separation of aqueous bioethanol. Carbon 2012; 50: 4220–4227. DOI: 10.1016/j.carbon.2012.05.003

[53] Wang CL, Hirade T, Maurer FHJ, Eldrup M, Pedersen NJ. Free-volume distribution and positronium formation in amorphous polymers: Temperature and positron-irradiation-time dependence. J. Chem. Phys. 1998; 108: 4654–4661. DOI: 10.1063/1.475876

[54] Pujari PK, Tashiro M, Tseng CY, Honda Y, Nishijima S, Tagawa S. Low-temperature positron studies in polymethylmethacrylate. Mater. Sci. Forum 2001; 363–365: 275–277. DOI: 10.4028/www.scientific.net/MSF.363-365.275

[55] He CQ, Dai YQ, Wang B, Wang SJ. Molecular weight effect on the microstructure and local motion in high molecular weight polymer observed by positrons. Mater. Sci. Forum 2001; 363–365: 309–312. DOI: 10.4028/www.scientific.net/MSF.363-365.309

[56] Stepanov AL. Nanofillers: Synthesis of metal nanoparticles in viscous polymer. In: Nicolais L, Borzacchiello A, editors. Wiley Encyclopedia of Composites. 2nd ed. Italy: Wiley; 2012. p. 1–9. DOI: 10.1002/9781118097298.weoc157

[57] Stepanov AL, Kiyan R, Ovsianikov A, Nuzhdin VI, Valeev VF, Osin YN, Chichkov BN. Synthesis and optical properties of silver nanoparticles in ORMOCER. Appl. Phys. A 2012; 108: 375–378. DOI: 10.1007/s00339-012-6894-6

[58] Stepanov AL. Synthesis of silver nanoparticles in dielectric matrix by ion implantation: A review. Rev. Adv. Mater. Sci. 2010; 26: 1–29. http://www.ipme.ru/e-journals/RAMS/no_12610/stepanov.pdf

[59] Takele H, Greve H, Pochstein C, Zaporojtchenko V, Faupel F. Plasmonic properties of Ag nanoclusters in various polymer matrices. Nanotechnology 2006; 17: 3499–3505. DOI: 10.1088/0957-4484/17/14/023

[60] Tuinstra F, Koenig JL. Raman spectrum of graphite. J. Chem. Phys. 1970; 53: 1126–1130. DOI: 10.1063/1.1674108

[61] Elman BS, Dresselhaus MS, Dresselhaus G, Maby EW, Mazurek H. Raman scattering from ion-implanted graphite. Phys. Rev. B 1981; 24: 1027–1034. DOI: 10.1103/Phys Rev B.24.1027

[62] Lee EH, Hembree DMJr, Rao GR, Mansur LK. Raman scattering from ion-implanted diamond, graphite, and polymers. Phys. Rev. B 1993; 48: 15540–15551. DOI: 10.1103/Phys Rev B.48.15540

[63] Ferrari AC, Robertson J. Interpretation of Raman spectra of disordered and amorphous carbon. Phys. Rev. B 2000; 61: 14095–14107. DOI: 10.1103/Phys Rev B.61.14095

[64] Ferrari AC. Raman spectroscopy of graphene and graphite: Disorder, electron-phonon coupling, doping and nonadiabatic effects. Solid State Commun. 2007; 143: 47–57. DOI: 10.1016/j.ssc.2007.03.052

[65] Morales GM, Schifani P, Ellis G, Ballesteros C, Martinez G, Barbero C, Salavagione HJ. High-quality few layer graphene produced by electrochemical intercalation and microwave-assisted expansion of graphite. Carbon 2011; 49: 2809–2816. DOI: 10.1016/j.carbon.2011.03.008

[66] Petrovski A, Dimitrov A, Grozdanov A, Andonovic B, Paunovic P. Characterization of graphene produced by electrolysis in aqueous electrolytes. In: Petkov P, Tsiulyanu D, Kulisch W, Popov C, editors. Nanoscience Advances in CBRN Agents Detection, Information and Energy Security. NATO Science for Peace and Security Series – A: Chemistry and Biology. The Netherlands: Springer; 2015. p. 103–110. DOI: 10.1007/978-94-017-9697-2_11

[67] Casiraghi C, Ferrari AC, Robertson J. Raman spectroscopy of hydrogenated amorphous carbon. Phys. Rev. B 2005; 72: 085401-1–085401-14. DOI: 10.1103/Phys Rev B.72.085401

[68] Matthews MJ, Pimenta MA, Dresselhaus G, Dresselhaus MS, Endo M. Origin of dispersive effects of the Raman D band in carbon materials. Phys. Rev. B 1999; 59: R6585–R6588. DOI: 10.1103/Phys Rev B.59.R6585

[69] Kavetskyy TS, Tsmots VM, Nowak J, Kuczumow A, Kinomura A, Kobayashi Y, Suzuki R, Mohamed HFM, Šauša O, Nuzhdin V, Valeev V, Stepanov AL. Comprehensive study of carbonization in B^+-implanted PMMA: A correlation between slow positron beam and Raman spectroscopy results. In: Proceedings of the 17th International Conference on Positron Annihilation (ICPA-17); 20–25 September 2015; Wuhan University; Wuhan; 2015. p. 45.

[70] Poly(methyl_methacrylate) [Internet]. 2016. Available from: http://en.wikipedia.org/wiki/Poly(methyl_methacrylate) [accessed 2016-01-28].